Ultrasonics - Sonochemistry 51 (2019) 20–30

Contents lists available at ScienceDirect

Ultrasonics - Sonochemistry

journal homepage: www.elsevier.com/locate/ultson

Urea functionalization of ultrasound-treated biochar: A feasible strategy for enhancing heavy metal adsorption capacity

Baharak Sajjadi[a,*], James William Broome[a], Wei Yin Chen[a], Daniell L. Mattern[b], Nosa O. Egiebor[c,1], Nathan Hammer[b], Cameron L. Smith[b]

[a] Chemical Engineering Department, School of Engineering, University of Mississippi, 134 Anderson Hall, Oxford, MS 38677-1848, USA
[b] Chemistry and Biochemistry Department, University of Mississippi, Coulter Hall, MS 38677, USA
[c] Environmental Resources Engineering Department, College of Environmental Science and Forestry (ESF), 206 Bray Hall, Syracuse, NY 13210, USA

ARTICLE INFO

Keywords:
Biochar
Ultrasound
Phosphoric acid
Urea
Amine functionalization
Heavy metal
Nickel

ABSTRACT

The main objective of a series of our researches is to develop a novel acoustic-based method for activation of biochar. This study investigates the capability of biochar in adsorbing Ni(II) as a hazardous contaminant and aims at enhancing its adsorption capacity by the addition of extra nitrogen and most probably phosphorous and oxygen containing sites using an ultrasono-chemical modification mechanism. To reach this objective, biochar physically modified by low-frequency ultrasound waves (USB) was chemically treated by phosphoric acid (H_3PO_4) and then functionalized by urea ($CO(NH_2)_2$). Cavitation induced by ultrasound waves exfoliates and breaks apart the regular shape of graphitic oxide layers of biochar, cleans smooth surfaces, and increases the porosity and permeability of biochar's carbonaceous structure. These phenomena synergistically combined with urea functionalization to attach the amine groups onto the biochar surface and remarkably increased the adsorption of Ni(II). It was found that the modified biochar could remove > 99% of 100 mg Ni(II)/L in only six hours, while the raw biochar removed only 73.5% of Ni(II) in twelve hours. It should be noted that physical treatment of biochar with ultrasound energy, which can be applied at room temperature for a very short duration, followed by chemical functionalization is an economical and efficient method of biochar modification compared with traditional methods, which are usually applied in a very severe temperature (> 873 K) for a long duration. Such modified biochars can help protect human health from metal-ion corrosion of degrading piping in cities with aging infrastructure.

1. Introduction

Biochars are carbon-rich materials produced through thermal decomposition, or pyrolysis, of organic matter in the absence of, or under a limited supply of, oxygen. The disordered aromatic sheets in chars generate incompletely saturated valences and unpaired electrons which provide active sites for adsorption, especially for polar and polarizable molecules (e.g. [1]). The ordered basal carbons of the aromatic sheet have high concentrations of delocalized π electrons and, thus, are considered Lewis bases [2] that can adsorb a large quantity of Lewis acids through reversible physisorption [3] and chemisorption [1]. The oxygen- and nitrogen-containing functional groups and minerals on biochar surfaces are the other active sites for adsorption that work through acid/base interactions and hydrogen-bond formation with adsorbates. Moreover, the presence of these functional groups makes biochar strongly hydrophilic, which allows graphene-like sheets to readily swell in water and increases the adsorption efficiency. These characteristics provide a natural adsorbent of substances harmful to the environment and humans, such as the greenhouse gas carbon dioxide and toxic heavy metals, which are the focus of this study.

Based on the literature, biochar can adsorb metal from an aqueous solution through six potential mechanisms including i) electrostatic interaction between a biochar surface and the adsorbing metal; ii) cation exchange between protons or alkaline metals on a biochar surface and the adsorbing metal; iii) complexation between functional groups and π-electron of biochar and the adsorbing metal; iv) co-precipitation to form insoluble compounds; v) inner-sphere complexation between hydroxy group [OH-] of a biochar surface and metal; and vi) physical adsorption. The sorption mechanism and capacity of adsorption are affected to a high extent by the target metals and biochar properties.

* Corresponding author.
E-mail address: bsajjadi@olemiss.edu (B. Sajjadi).
[1] Formerly with Chemical Engineering Department, School of Engineering, University of Mississippi, 134 Anderson Hall, Oxford, MS 38677-1848, USA.

https://doi.org/10.1016/j.ultsonch.2018.09.015
Received 28 February 2018; Received in revised form 7 September 2018; Accepted 15 September 2018
Available online 17 September 2018
1350-4177/

Table 1
A summary about different methods of nickel removal.

Method	Initial Conc. (mg/L)	Residual Conc. (mg/L)	Removal Efficiency %	Comment	Ref
Hydroxide Precipitation *mixture of metals	1.9	0.3	84.2	pH limited and can have an adverse effect on some metals. Hard to filtrate.	[50]
Carbonate Precipitation	26	1.18	95.4	No advantage to hydroxide precipitation for ease of operation	[50]
Coagulation/ Flocculation	2.8	0.9	68	Limited usage and pH dependent	[50]
Ion Exchange	8.9	0.16	98.2	High cost and complicated operation. High chemical cost and chemicals must be removed.	[50]
Liquid Ion Exchange	100	< 1	> 99	Hard to concentrate metals.Complicated system.	[50]
Biological Operations	–	–	60–90 *7–8 pH	pH dependent.	[50]
Membrane Operations	–	–	90–97	High cost and very limited operation. Membranes don't last, composite membranes are expensive.	[50]
Electrocoagulation	25	< 1	> 99	Constant power consumption and pH dependent	[51]
Activated Carbon	30	7.5	Max 75	Can adsorb over a broader range of pH, but low absorption percentage, expensive compared to biochar	[52]

The groups and structures associated with biochar depend on its phase of charring. For example, biochars produced at temperatures over 773 K have higher surface area and porosity and are better for adsorbing inorganic pollutions, while biochars produced under 773 K have higher oxygen functional groups and are better for adsorption of heavy metals [4].

Among the heavy metals, nickel is commonly observed in drinking water due to corrosion of pipes. Ni(II) ion in drinking water is in the form of $Ni(H_2O)_6^{2+}$. Although the Ni(II) ion is not deadly unless many grams of the salt are digested, it may cause allergic reactions in long-term uptake and a high-level uptake increases the chance of developing lung cancer, prostate cancer, larynx cancer, heart disorders, chronic bronchitis, and asthma [5]. This creates a need to remove Ni from the soil, industrial wastewater, effluents, and drinking water. Table 1 summarizes the current methods applied for treatments of waters containing Ni(II). Most of these methods have been used in waters containing a low concentration of Ni(II). Moreover, some of those methods are not economically sound, due to high power consumption, expensive materials, and intricate removal methods that operate under specific pH levels. A few of the methods have very high removal efficiencies, but they lack affordability or are limited to certain environments. Biochar's reasonable removal efficiency and cost-effectiveness give it advantages over other methods to rid waste and drinking water of heavy metals. However, biochar's adsorption capacity is significantly influenced by the homogeneity of the structure, uniformity of surface, types of functional groups, and the contact surface between adsorbate/adsorbent. Non-homogeneity of the structure and non-uniformity of the surface due to defects and unsaturated sites limit access to many potential active sites and reduce the adsorption capacity [6]. Biochar also has ash and many unneeded minerals attached to the surface and pores. If the pores and surface are cleaned of unwanted materials, the char can adsorb more materials. The surface can also be functionalized with groups that further adsorb specific substances. Hence, biochar produced from thermal decomposition processes is often physically and chemically activated to increase its specific surface area, porosity, pore size distribution, and to attach a number of desired functional groups. Ultrasound irradiation is an effective method for modification of different structures. Physical effects of ultrasound on plant materials have been identified as erosion (of plant structure), fragmentation (reduction of particle size), sonocapillary effect (increase of solvent penetration into canals and pores of plant material), local shear stress (streaming and microstreaming effects), detexturation (destruction of plant structures) and sonoporation [7]. *Sonoporation*; ultrasound-induced membrane *porosity,* is being extensively studied as a promising technique to facilitate gene/drug delivery to cells [8]. Microbubbles play a vital role in the process of sonoporation. In short, gas-filled micro-bubbles are compressible and hence they can respond to the ultrasound pressure waves by alternate growing and shrinking. High ultrasound intensities, may finally lead to microbubble implosion and formation of micro-jet [9]. This process is named cavitation which propels the process of sonoporation resulting in formation short-lived, non-specific pores on cell membranes [10]. This process can also be applied on the other structures to form stable pores and increasing their permeability [11]. The effect of ultrasound on graphene oxide layers was first discovered by Stankovich et al. [12]. They found that a mild ultrasonic treatment (f_c = 78.6 kHz, 150 W) of graphite oxides in water for 1 h exfoliates the layers and forms stable aqueous dispersions that consist almost entirely of 1-nm-thick sheets [13]. It also breaks apart C—C bonds in carbon materials, while also promoting transformations like nanotube and diamond synthesis [14]. Inspired by Stankovich's study, Chen et al. [15] investigated sonochemical routes in the reactions between carbonaceous compounds and (CO_2 + H_2O) mixtures. The authors found that ultrasound induces a group of synergistic processes during sonotreatment of biochar in CO_2 and H_2O, including exfoliation of GO and graphite clusters, mineral leaching, hydrogenation, and chemisorption of CO_2 on biochar. All these phenomena happen simultaneously and cause a 50.3% increase in the heating value of the biochar. As a sequel to our previous work, this study for the first time investigates the potentiality of ultrasound energy in physical modification of biochar and its synergistic interaction with chemical functionalization. Ultrasound provides a time- and energy-reducing method that can easily be applied to large-scale processes without releasing harmful gases [16]. The main objective is to take one step toward industrializing the applications of ultrasound in biochar activation and to develop a new and efficient activation strategy that consumes lower energy and takes a shorter time compared with the current activation methods.

2. Materials and methods

2.1. Material

Biochar-Now company (Berthoud Colorado, U.S.A.) supplied raw biochar for the experiments. The feedstock used for this biochar is softwood pine. Pyrolysis of the biomass is accomplished at temperature between 823 and 873 K in an oxygen-deprived environment in a kiln reactor with a multi-zone combustion chamber. After pyrolysis, the biochar is exposed to nitrogen to stop the process. The activating acid, phosphoric acid (H_3PO_4, 85%), the functionalization chemical urea (CH_4N_2O, > 98%, powder), and the heavy metal to be adsorbed, nickel ($NiCl_2$, 98%, powder), were purchased from Sigma-Aldrich. All water mixed for dilutions was deionized water (Walmart).

2.2. Biochar activation

2.2.1. Synthesis

Particle size plays a key role in adsorption capacity. In this study,

raw biochar was first sieved to have particle sizes between 0.125 and 0.85 mm. For each experiment, three grams of raw biochar were slightly mixed with deionized water and bubbled with CO_2 for 30 min. The mixture was then placed in a glove box (which had been purged three times with CO_2), and lightly stirred by a stirring rod for another 10 min. It was then subjected to ultrasound by a 20 kHz-ultrasonic processor (Qsonica, model no. XL2010) at 100% amplitude for 20, 40, or 60 s (which consumes 1787, 3583 and 5600 J energy, respectively), still in a CO_2 atmosphere. The ultrasono-modified biochar (US-BC) was then separated from the mixture by simple filtration, allowed to vacuum dry overnight at 333 K, and sieved in air between mesh No. 100 and 60. The particle sizes reduced to 0.149–0.25 mm after ultrasound irradiation. US-BC was then chemically treated with 25%, 50%, or 85% phosphoric acid solutions at 323 K for 3 h, washed with deionized water, and dried under vacuum. Once physically and chemically treated, the biochar was functionalized with different molarities of urea (0.5, 1.0, 3.0, 6.0, or 10.0 Molar in water) as follows: one gram of US-BC was added to 5 mL of urea solution and the mixture was placed in an oscillator at room temperature for 8 h, then filtrated, washed with deionized water to remove any unreacted urea, and dried under vacuum overnight at 333 K. Deionized water was produced in our own laboratory. In this system, water passes through two types of ion-exchange sites; including positively charged ions (cations) and negatively charged ions (anions) and becomes free of negative and positive ions. The produced deionized water has a *pH*-value of approximately 7 (6.4–7). This slight variation has not had any effect on our experiments since CO_2 bubbling in the first step of activation, further reduced the pH to around 5.3–5.6. Phosphoric acids of different concentrations were prepared by dilution of the main chemical and molar-based solutions of urea were separately prepared by dissolution of the specific weights of urea in deionized water. Solutions were mixed well on hot plate to reach the desired temperature before adding the ultrasound-treated biochar.

Accordingly, three subsequent steps were applied for activation of biochar after CO_2 bubbling: i) Physical activation under different duration of ultrasound irradiation (0, 20, 40 and 60 sec), ii) chemical treatment using different concentration of phosphoric acid (0, 25%, 50% and 80%), iii) chemical activation using different concentration of urea (1, 3, 6 and 10 M). 12 different combinations of the mentioned activation processes including (US20, P0%,UR0M), (US40, P0%,UR0M), (US20, P50%,UR6M), (US40, P50%,UR6M), (US20, P0%,UR6M), (US20, P25%,UR6M), (US20, P50%,UR6M), (US20, P85%,UR6M), (US20, P50%,UR1M), (US20, P50%,UR3M), (US20, P50%,UR6M) and (US20, P50%, UR10M).

2.2.2. Characterization

Micro- and macroporosity of the activated biochar was characterized by a surface area pore size analyzer (Quantachrome 2000E series). CO_2 and N_2 were used to test adsoption/desorption for the micro and macro-porosity, respectively, as well as the corresponding surface area. BET-N_2 and DR-CO_2 both were conducted using Quantachrome Nova 2000e series BET analyzer. Prior to analysis the samples were degassed at 573 K for 3 h. Analysis was done with liquid nitrogen bath at temperature -196.15 K for macroporous surface area analysis using BET equation. For micro and mesoporous surface area, analysis was done with ice-water bath at −273.15 K using DR equation. Scanning Electron Microscopy (SEM) was used to investigate the surface structure of the raw and the modified biochar. Surface functional groups of the modified biochar were characterized by Fourier-Transform Infrared Spectroscopy (FTIR), and the graphitic structure of biochar under different activation conditions was analyzed using Raman spectroscopy. FTIR was conducted using Cary 660 FTIR (Agilent) instrument. Samples were dried at 333 K under vacuum prior to analysis. Background scan was conducted before each sample is scanned. Samples were put in ATR crystal and scanned in the wavelength range of 400–4000 cm^{-1}. Raman spectra were acquired using a Horiba LabRAM HR Evolution Raman spectrometer system in air at room temperature using a 532-nm wavelength laser. The laser was focused onto the sample using a 100X objective. The quantities of organic elements (C, N, O, H), as well as ash content, were investigated by elemental analysis (Huffman Hazen Laboratory, Colorado). Different elements of biochar were determined by dry combustion in which elements such as carbon, hydrogen, nitrogen and oxygen are converted to simple gasses of CO_2, H_2O, N_2 and CO, respectively. The product gasses are then separated under steady state conditions and measured as a function of thermal conductivity.

2.3. Ni(II) removal

Adsorption experiments were conducted in a conical flask placed in an oscillator. In each set of experiments, 0.5 g of activated biochar was added to 50 mL of 100 mg/L Ni(II) solution and the mixture was stirred for different amounts of time. All tests were conducted under atmospheric pressure and 295 K. The mixture was then filtered and the filtrate was analyzed by UV–visible spectrophotometry. In aqueous solution, nickel (II) ion forms from either nickel(II) chloride solution $NiCl_{2(aq)}$ or nickel(II) sulfate $NiSO_{4(aq)}$. The chemistry of nickel is dominated by the +2 oxidation state. Nickel(II) can make different complexes with different compounds e.g. ammonia, sodium carbonate, etc. These complexes generate solution of different colors. In water nickel forms a green stable hexaaqua nickel (II) ion, $[Ni(H_2O)_6]^{2+}_{(aq)}$. The intensity of the color depends on the concentration of the hexaaqua nickel (II) complex which can be further analyzed through Ultraviolet–Visible spectroscopy. The wavelength selection depends on the color of the solution. In this study, the best results were obtained by using the wavelength of 530 nm, which is in the region of green color in visible light spectrum. Moreover, prior to the experiments, the UV–Vis (Hach DR 6000) was calibrated with different Ni(II) concentrations and then the Ni(II) concentrations were measured as per the calibration curve.

3. Results and discussion

3.1. Physical activation of biochar under ultrasound irradiation

Specific surface area and porosity are among the most important characteristics of carbonaceous materials. They not only affect the adsorption capacity of the adsorbents, but also play key roles in chemical activation and functionalization. An appropriate pore size distribution provides suitable channels for chemical compounds to approach the lower layers for grafting new functional groups onto the carbonaceous structure. The pore size distributions and specific surface areas of biochars treated with ultrasound are summarized in Table 2. The micropore surface area of the biochar, as analyzed by CO_2 as the adsorbate, showed a slight increase from 347 to 389 m^2/g after exposure to 20 s of ultrasound. Afterward, additional ultrasound time did not cause a significant increase in surface area. A different trend was observed in the macro-meso surface area, as determined by N_2 adsorption isotherms at −196.15 K; this surface area decreased with each additional

Table 2
Micro and macro porosity of raw and ultrasono-modified biochar.

Biochar ID	Sonication Time (s)	Energy (J)	Micro-Porosity		Macro & Meso Porosity	
			DR Surface Area (m^2/g)	Porosity (cc/g)	BET Surface Area (m^2/g)	Porosity (cc/g)
Raw	0	0	347.024	0.096	69.055	0.050
US-B20	20	1787	389.608	0.108	54.074	0.042
US-B40	40	3583	383.530	0.128	34.304	0.028
US-B60	60	5600	392.937	0.131	26.641	0.023

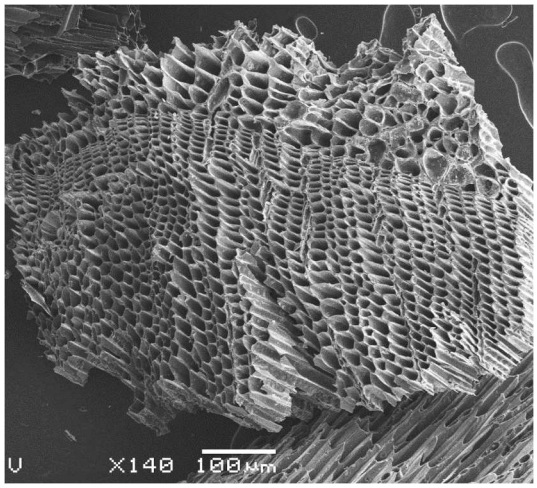

Fig. 1. Cross-sectional Microscopic surface scan of the raw biochar.

application of ultrasound. The microporosity of biochar consistently increased with added ultrasound time with about 10% increase in porosity per 20 s of sonication, while the macro- and mesoporosity showed a significant and consistent reduction.

Aside from the effect of ultrasound in cleaning the surface of biochar, one reason for these observations relates to the origin of macro- and mesopores. When biochar is exposed to cavitation induced by ultrasound, the generation of new micropores, or the opening of blocked ones, increases its microporosity and reduces its macro- and mesoporosity. These changes in the surface morphologies of raw and sonicated biochar were revealed by SEM imaging (Figs. 1 and 2). As observed, the surface textures of the raw biochar were comparatively rough and uneven. We also noted that unmodified biochar contained some white/gray lumps deposited on the surface, as shown by blue curves in Fig. 2a. After exposure to ultrasound, a significant number of circular pores, ranging from 2 to 3 µm, developed on the surface of the biochar (Fig. 2b). The porosities observed mainly correspond to the removal of the lumps in the original structure of biochar (Fig. 2a). This implies that cavitation dislodged a portion of those lumps on the biochar surface. These lumps could be the residues of pyrolysis products which significantly blocked the pores, leading to a reduced surface area and porosity. Similar observations have been reported by other authors [17–19]. Hamid et al. [17] observed that a one-step carbonization at 673 K failed to create sufficient porosities in biochar due to incomplete decomposition of organic constituents present in the carbonaceous precursors. Therefore, the authors catalyzed the formation of circular pores with KOH solution in the presence of CO_2 at 373 K for 6 h, followed by a secondary pyrolysis at 973 K for 2 h. In another study, Wan et al. [19] reported the development of a porous structure with several pits after a two-step pyrolysis, first at 773 K for 1 h and then at 1273 K for 2 h.

3.2. Chemical activation of biochar

Recent achievements have demonstrated that phosphoric acid (H_3PO_4) can be used as a mild activation agent on various forms of carbon. High temperatures (> 1023 K) can lead to the oxidative destruction of the carbon framework, with reduction of phosphorus as follows: $4H_3PO_4 + 10C \rightarrow P_4 + 10CO + 6H_2O$ [20]. At temperatures between 723 K and 1073 K, significant improvements can also occur in pore quantity and surface area [21]. With thermal treatment at < 373 K, H_3PO_4-activated biochar has been used to remove pesticides from contaminated water, through π-π dispersive interactions and H-bonding from the phosphate OH groups to highly polar bonds in the pesticides [22]. H_3PO_4 treatment of chars can improve properties such as the adsorption of dyes [23] or metal ions like Cu from water, [20] or

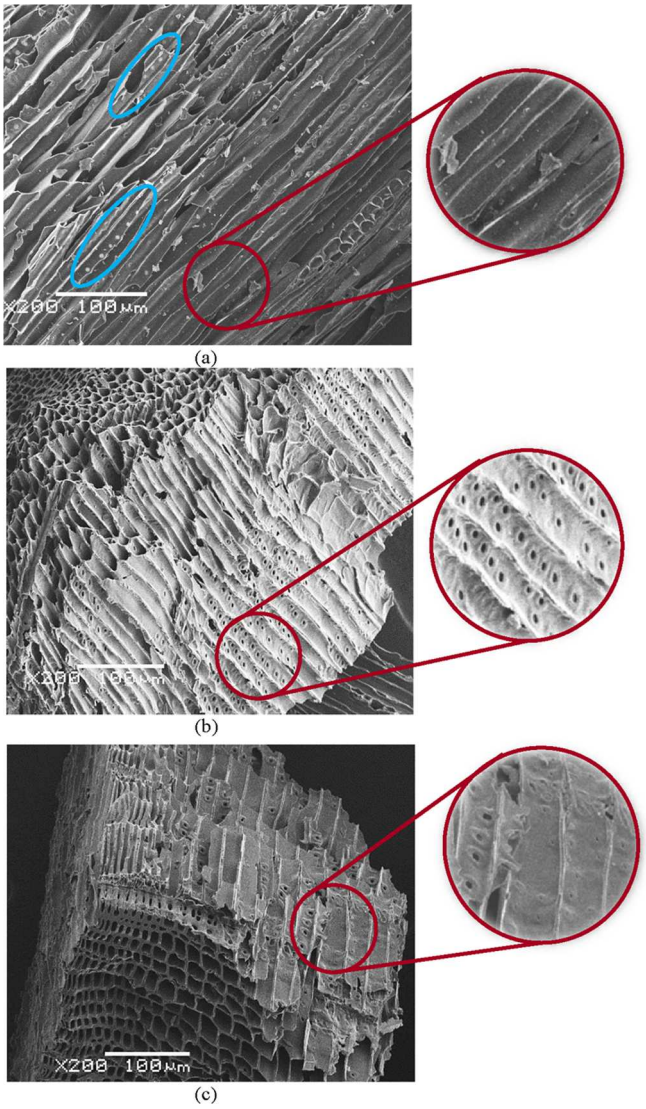

Fig. 2. Microscopic surface scan of biochar of a) raw biochar, b) ultrasound treated biochar, c) ultrasound treated-urea functionalized biochar.

graphene's electrical capacitance. [24]. It has been reported that phosphorus-containing structures (such as P = O or P = OOH) can form complexes with metal ions that cause enhanced sorption of Ni(II) and Cu(II) [25]. Uchimiya et al. [26] indicated that the ability of phosphoric acid-activated carbons to sorb heavy metals increased linearly with the content of oxygen containing functional group and most authors concluded that PO_4^{3-} in biochar participates in heavy metal ions removal [27,28].

$$2{-}POOH + M^{2+} \rightarrow (-POO)M + 2H^{+} \quad (1)$$

$$-R{-}OH + M^{2+} \rightarrow -R{-}OM^{+} + H^{+} \quad (2)$$

SEM images show that such H_3PO_4 treatment increases porosity and dissociates weakly bonded components (e.g. labile carbon and volatile matter) from the biochar surface [29]. Treatment of graphene oxide (GO) with H_3PO_4 and polyphosphoric acid at < 373 K results in a phosphonated GO which can be used as a catalyst; the deconvoluted XPS spectrum for carbon suggested the presence of C—P bonds in the activated GO [30]. The XPS spectrum from a similar study by Some et al. [31] of phosphonated GO (used as a flame retardant) could be interpreted without assuming C—P bonds, but the XPS indicated about 20 atom% P in the sample, suggesting a covalent attachment of phosphate to either O or C. Possible modes of this covalent attachment to

biochar (or GO) frameworks are suggested by the reactions below. Reaction (1) is the nucleophilic opening of an epoxide by phosphate, followed by dehydration to make a phosphate ester. Reaction (2) shows a direct esterification of a phenolic hydroxyl group to the same ester, a dehydration process that would be expected to be reversible. The direct phosphorylation of an aromatic ring by electrophilic aromatic substitution has been demonstrated with the reactive reagent phosphorus pentoxide, [32] but $(P_2O_5)_2$ is not stable in water. Some et al. proposed Reaction (5) as a way to provide electrophilic phosphate from polyphosphoric acid [31]. This would provide the C—P bond suggested by XPS, while making a stable aryl phosphonate. Some et al. also reported that phosphonation resulted in an expansion of the interlayer distance in the activated GO, making internal pores and surface more accessible to potential adsorbants [31]. Therefore, H_3PO_4 treatment is expected to improve the performance of biochar in adsorbing inorganic contaminants via adsorption to its surface, which should be strongly negative at pH > 3.

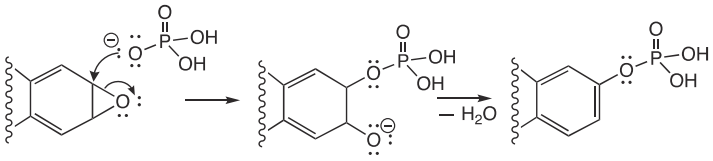

(3)

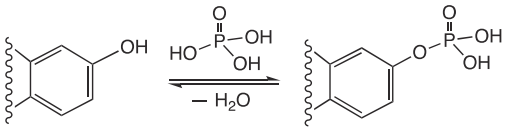

(4)

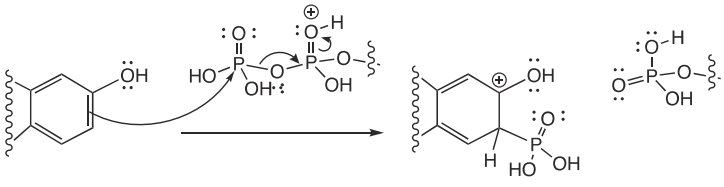

(5)

Urea, $CO(NH_2)_2$, is an alternative modifying agent that can be used to load N functional groups onto carbonaceous materials. For example, activated carbon treated with urea had improved adsorption of Pb(II) [33]. Urea contains one carbonyl (C═O) and two amino (−NH_2) groups that allow hydrogen bonding to hydroxyl, carboxylic, or phosphoric acid groups, as shown in (6).

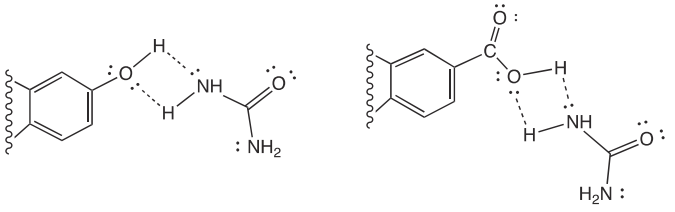

(6)

Prior activation with H_3PO_4 thus provides a way to increase the complexation of urea to the biochar. For example, modification of activated carbons with H_3PO_4 followed by urea improves its adsorption capacity towards Cd(II). As an alternative, treatment of a biomass with urea phosphate before charring also provides an excellent Cd(II) adsorbant [34]. The ability of amino functional groups to easily bind with heavy metals is well known [35,36]. Naowanon et al. [35] found that amine functionalization could increase the Cu(II) and Fe(II) adsorption capacity of silica nanoparticles from 21.74 to 27.03 and from 25 to 83 mg/g, respectively. Similar results have been reported in cases of Ni (II), Pb(II), Cd(II), and Zn(II) [37]. The adsorption mechanism of a heavy metal by amine groups is as follows [36,38]:

$$R{-}NH_2 + H^+ \rightleftarrows R{-}NH_3^+ \quad (7)$$

$$R{-}NH_3^+ + M(II) \rightarrow R{-}NH_2M(II) + H^+ \quad (8)$$

$$R{-}NH_2 + M(II) \rightarrow R{-}NH_2M(II) \quad (9)$$

Aside from the adsorption capacity of the biochar, which is significantly increased by physiochemical modification, the adsorption process became remarkably faster due to the advent of amino functional groups that can easily bind to heavy metals. Faster adsorption of trace metals due to the presence of amino groups has been reported by the other authors as well. As an example, Aguado et al. [37] used amino functionalized mesoporous silica SBA-15 materials for removing the trace metals of Cu(II), Ni(II), Pb(II), Cd(II), and Zn(II), and found that a high quantity of metal was quickly removed in the early stages of the process.

Urea decomposition is also an important process. When heated in aqueous solution above 423 K, urea decomposition yields cyanate (CNO^-) and ammonium (NH_4^+) ions; further heating gives further decomposition gasses. [27] These gasses have reducing power, and are able to deoxygenate GO, converting it to a more graphene-like structure [39]. Ammonium formed in this way can associate with anionic carboxylate, phosphate, or phosphonate groups on biochar, and NH_3 also intercalates between GO layers.

3.3. Characterization of physiochemical modified biochar

3.3.1. Effect of modification on elemental composition of biochar

The effects of phosphoric treatment, urea functionalization and ultrasonication on the modified biochar were shown by elemental analysis of the organic elements C, N, O, and S, as well as a determination of the ash content (Table 3). Since the ash content varied widely, we also calculated the elemental composition of the organic material alone,

Table 3
Elemental composition of raw and modified biochar under different conditions.

Biochar ID	Carbon % w/w	Hydrogen % w/w	Nitrogen % w/w	Oxygen % w/w	Sulfur % w/w	Ash % w/w
Raw Biochar	65.36	1.97	0.18	11.22	0.05	23.95
US20-P50%-U1M	68.33	2.19	0.88	11.54	0.03	16.63
US20-P50%-U3M	62.05	2.13	1.13	11.18	0.02	24.69
US20-P50%-U6M	**58.22**	**2.03**	**1.56**	**10.74**	**0.03**	**28.25**
US20-P50%-U10M	63.48	2.25	2.19	11.94	0.02	20.51
US 0-P50%-UR6M	59.84	2.16	2.85	11.51	0.06	24.41
US20-P50%-UR6M	**58.22**	**2.03**	**1.56**	**10.74**	**0.03**	**28.25**
US40-P50%-UR6M	61.85	2.12	1.41	11.07	0.04	24.61
US20-P0%-UR6M	49.53	1.83	1.60	10.05	< 0.01	39.80
US20-P25%-UR6M	48.24	1.80	1.20	9.94	0.01	41.10
US20-P50%-UR6M	**58.22**	**2.03**	**1.56**	**10.74**	**0.03**	**28.25**
US20-P85%-UR6M	64.47	2.28	1.45	12.28	0.02	21.70

The bold values are related to the “control test”.

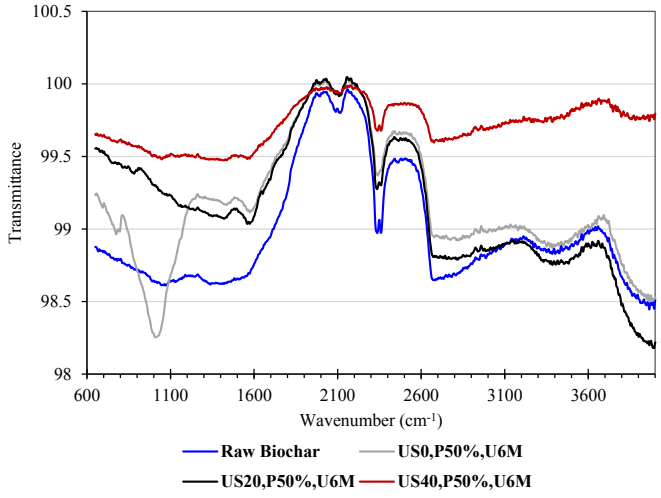

Fig. 3. The effect of sonication duration on FTIR analysis of raw biochar and ultrasono-phosphoric acid treated/urea functionalized biochar.

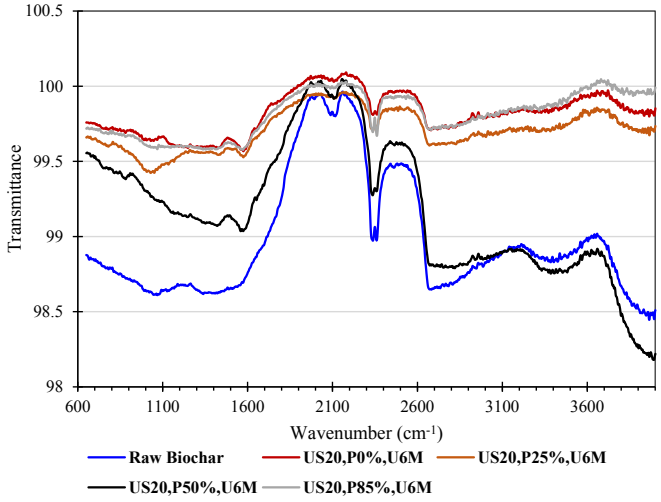

Fig. 4. The effect of phosphoric acid concentration on FTIR analysis of raw biochar and ultrasono-phosphoric acid-treated/urea functionalized biochar.

omitting the contribution of ash; this is shown in Table 3A of the Supplementary Materials.

The first block of Table 3 shows the elemental characteristics of raw biochar. The second block demonstrates the effect of increasing urea concentrations for biochar samples activated with 20 sec of ultrasound and 50% phosphoric acid. There was a consistent reduction of carbon content of the modified biochar with increasing urea concentration, consistent with the low %C of urea (20.0%). This relationship is clear in Table 3A, although the very low ash content of US20-P50%-U1M muddles the trend in Table 3. As the urea concentration increased, the %N incorporated, representing adsorbed urea, increased steadily. Even the 1 M urea sample showed significant incorporation of N. Both oxygen and hydrogen increased with urea concentration, again consistent with their elevated presence in urea, but these trends are not as significant as with the N content. This could reflect displacement of water from adsorbed sites on the char, or from hydrogen-bonding networks, by urea or ammonia from urea decomposition.

The focus of block 3 is on the role of ultrasound. A small reduction was observed in the nitrogen content of biochar with increasing sonication time, which could be due to lower macro- and mesoporosities in those samples. This suggests that macroporosity is more favorable for urea attachment than microporosity. The other two important points are related to oxygen and carbon content. Our previous studies showed that sonication of biochar under CO_2 bubbling resulted in attaching more carbon atoms to biochar, while oxygen atoms were rejected. Those results were confirmed here once more. Comparing US0-P50%-UR6M and US40-P50%-UR6M, which have similar ash content, the %O reduced in biochar sonicated for 40 s compared with no sonication, and the %C increased. The trend with all three samples is shown clearly in Table 3A.

The effect of phosphoric acid concentration is presented in the fourth block of the table. The effects on organic composition were small. This can be seen by comparing samples US20-P0%-U6M and US20-P25%-U6M, which have similar ash content. US20-P0%-U6M was functionalized without H_3PO_4. Addition of 25% phosphoric acid increased the oxygen content from 14.24 to 16.24% (Table 3A). Incorporation of phosphates should increase the %O because of the large %O in H_3PO_4. Using higher concentrations of H_3PO_4 did not, however, appear to lead to higher incorporations.

In terms of ash content, the elemental analysis suggested the ash content was maximal with a urea concentration of 6 M, and above that, it decreased. Moreover, the highest ash contents were observed in the samples with 0% and 25% phosphoric acid, and ash decreased as the H_3PO_4 concentration increased, suggesting a role for phosphoric acid in removing ash. There did not seem to be a big effect of ultrasound duration on ash content.

3.3.2. *Effect of modification on functional groups of biochar*

Figs. 3–5 show the FTIR spectra of raw biochar compared with those treated under different sonication durations, phosphoric acid concentrations, and urea molarities. In these figures, the strong and sharp peaks at 2350 point to the CO_2 stretching vibration. The strong and

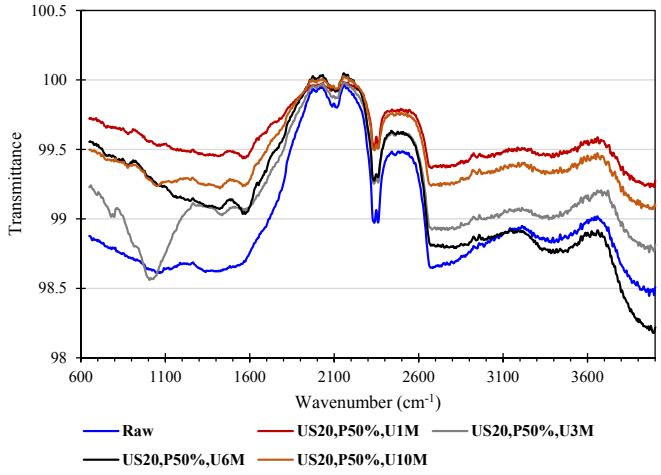

Fig. 5. The effect of urea concentration on FTIR analysis of raw biochar and ultrasono-phosphoric acid-treated/urea functionalized biochar.

wide peak between 3300 cm^{-1} and 3600 indicates the stretching of surface OH groups [40] in raw biochar. It should be noted that this region also corresponds to the NH stretching vibration in amino compounds. Consistently, the peak at 3300–3600 cm^{-1} reduced in all treated biochars except for US20-P50%-U6M. The small peak at around 1420–1460 corresponds to the asymmetric scissoring vibrations of N-C-N and the band at 1586 cm^{-1} is mainly due to the bending mode of NH_2. Neither of these peaks existed in raw biochar but were clearly observed in urea functionalized biochar. The advent of these peaks due to urea functionalization was also observed in magnetic-urea-activated carbon sorbent which was synthesized for removal of uranium (VI) from aqueous solution [41].

3.3.2.1. Effect of phosphoric acid. The effect of phosphoric acid is presented in Fig. 4. The FTIR spectrum of biochar functionalized without phosphoric acid showed a significant removal of oxygen functional groups due the reductive ability of urea [42]. Pretreatment of biochar with diluted phosphoric acid (25%) gradually increased the intensities of OH-related peak at 3300–3600 cm^{-1}. The highest intensities of both OH and NH_2 related peaks were observed in sample treated with acid concentration of 50%. Consistent with FTIR result, elemental analysis showed the maximum N content of 1.56% in Table 3 and 2.15% in Table 3A for the sample of US20-P50%-UR6M. However, a very high concentration of phosphoric acid (85%) appeared to reduce the intensity of surface OH groups, which is more aligned with the organic elemental analysis (Table 3A).

It is known that phosphoric acid dissociates weakly bonded

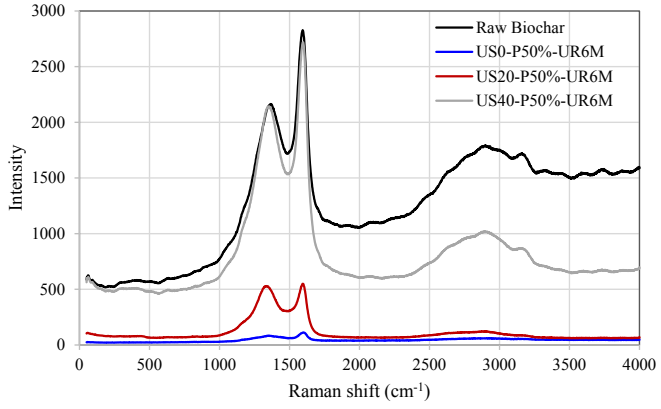

Fig. 6. Raman spectra of raw and the modified biochar using different ultrasound durations.

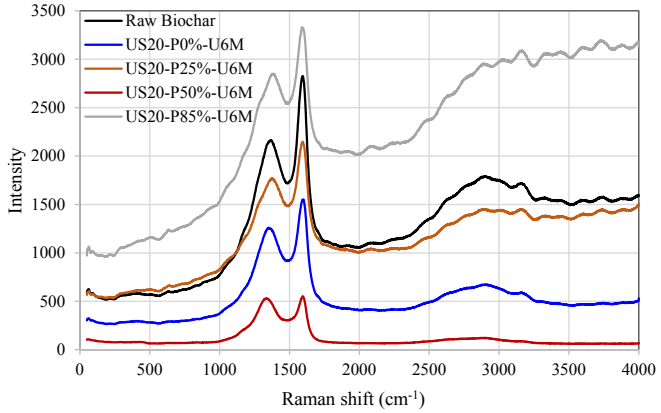

Fig. 7. Raman spectra of raw and the modified biochar using different concentrations of phosphoric acid.

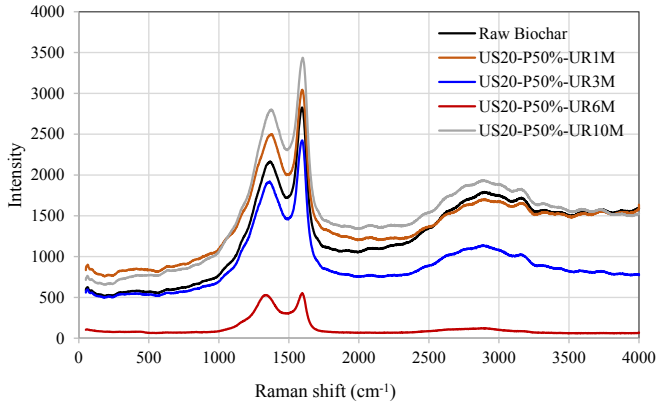

Fig. 8. Raman spectra of raw and the modified biochar using different concentrations of urea.

components from the particle surface, [20] which could be the reason for ash content reduction. On the other hand, a portion of the carbon may be functionalized by phosphoric acid, creating new groups on the surface and inside the pores which was also suggested by the increasing intensity of OH group (as per IR results) with phosphoric acid concentration to 50%. In this study, the process was followed by urea functionalization. Urea may remove some of oxygen containing groups and may react with some others. That's why the oxygen content of the modified biochar in samples with different phosphoric acid concentrations did not follow a unique trend. For example, the small peak at 890 cm^{-1} in US20-P50%-U6M could be related to P-O-P stretching,

Table 4
Graphitization degree of raw and modified biochar.

Biochar ID	ID/IG
Raw Biochar	0.766
US20-P50%-U1M	0.821
US20- P50%-U3M	0.793
US20- P50%-U6M	**0.963**
US20- P50%-U10M	0.816
US 0-P50%-UR6M	0.749
US20-P50%-UR6M	**0.963**
US40-P50%-UR6M	0.789
US20-P0%-UR6M	0.813
US20-P25%-UR6M	0.825
US20-P50%-UR6M	**0.963**
US20-P85%-UR6M	0.866

The bold values are related to the "control test".

but this peak was not observed in other samples [43]. The role of phosphoric acid in formation of P-containing groups will be investigated in our next coming work.

3.3.2.2. Effect of urea. On the other hand, the intensity of NH_2 peak at around 1586 cm^{-1} gradually increased with urea concentration up to 6 M (Fig. 5) which followed the same trend of elemental analysis. These results demonstrated the successful doping of N atoms into the biochar structure. Consistent with this, the intensity of OH peak slightly increased with urea concentration of 6 M. Further increase of urea reduced the intensity of both NH_2 and OH peaks. This could reflect the reductive ability of urea which was intensified at the maximum concentration of 10 M.

3.3.3. Effect of modification on graphitic structure of biochar

The Raman spectra of raw and the activated biochar using different treatments are demonstrated in Figs. 6–8. Generally, the two prominent peaks around 1360 and 1597 cm^{-1} are assigned to the D band (sp^3-hybridized carbon atoms) and the G band (ordered graphitic sp^2-hybrid carbon atoms), respectively, and the clear 2D band at around 2800 cm^{-1} corresponds to the multilayer graphene-phase structure. In simple words, the D band relates to the presence of amorphous or disordered carbon and defects in carbon structure, while G band relates to the more organized, less defective graphene structures. The intensity ratio of the D to G bands (I_D/I_G) describes the graphitization degree of carbon materials in that the higher the I_D/I_G ratio, the lower the graphitization degree. As observed, the ID/IG of raw and the modified biochars (Table 4) are between 0.766 and 0.963 which shows graphitization level is much smaller than graphite materials. It should be noted that the level of graphitization in biochars depends on the pyrolysis temperature. At low temperatures (100–200 °C), biomass is mainly dehydrated and remains almost unaltered. Three distinct phases of biochar are formed which are known as transition biochar, amorphous biochar, and composite biochar with gradual increase of pyrolysis temperature from 373 to 973 K, respectively. As soon as all amorphous organic C is either converted into aromatic rings or volatilized, a new phase is recognized as 'carbonized' or 'turbostratic'. Biochars do not usually get to this region as they either require heating temperatures beyond 973 K or prolonged residence during pyrolysis. Hence, most biochars have a highly disordered and heterogeneous carbon structure (belonging to either amorphous or composite categories) [44,45]. Softwood pine biochar used in this study has also been pyrolysed at temperature between 823 K and 873 K. Therefore, although its ID/IG is much higher than graphite materials (Graphitization is lower), but the value is comparable with the ID/IG of common bicohars [46,47].

According to the results (Table 4), I_D/I_G of the raw biochar was 0.766 while the value significantly increased in all ultrasono-modified biochars, indicating the presence of more sp^3 bonds and more transitions from sp^2 to sp^3 material, meaning that more induced defects and disorders were created in the modified biochars [48]. In contrast, I_D/I_G slightly reduced to 0.749 in the sample directly oxidized with acid and functionalized with urea without any ultrasound treatment (US0-P50%-U6). The elemental analysis showed that this sample had the highest hydrogen content and a much lower carbon content but similar oxygen and ash content compared with the raw biochar. So the lower I_D/I_G value may be attributed to the role of urea in removing defected carbons. The broader D band of the raw biochar also suggested the presence of oxygen functional groups that led to reduced size of the sp^2 domain of biochar by creating defects and distortions [48]. The high I_D/I_G (0.96) obtained in the sample treated with 20 sec of ultrasound, 50% phosphoric acid, and 6 M urea is likely due to a large inventory of defects, wrinkles, and new functional groups on the carbonaceous structure. Further exposure to ultrasound waves up to 40 sec reduced the ratio to 0.78, probably due to the smaller number of functional groups on the modified biochar. Meanwhile, the I_D/I_G ratios for biochars activated with 0%, 25%, 50%, and 85% phosphoric acid (with 20 sec of ultrasound and 6 M urea) were 0.813, 0.825, 0.963, and 0.856, respectively, which implied that elevating phosphoric acid up to 50% was beneficial for creating new functional groups. However, it should be noted that the infrastructure of this potential had been prepared by the ultrasound irradiation through exfoliating and disordering the graphene-like sheets, making more layers accessible to the phosphoric acid [12]. Although this enhancement is higher than others it is reasonable compared with the increase of ID/IG from 0.76 in raw biochar to 0.85 in US20-P85%-U6M. On the other hand, the sample of US20-P85%-U6M showed the highest removal of heavy metal. Therefore, a difference is expected in its structure compared with the other samples. Moreover, this difference in ID/IG which is mainly due to the synergism interaction between the concentrations of phosphoric acid and urea during treatment and functionalization demonstrate the presence of an optimum point in this range of the chemical concentrations.

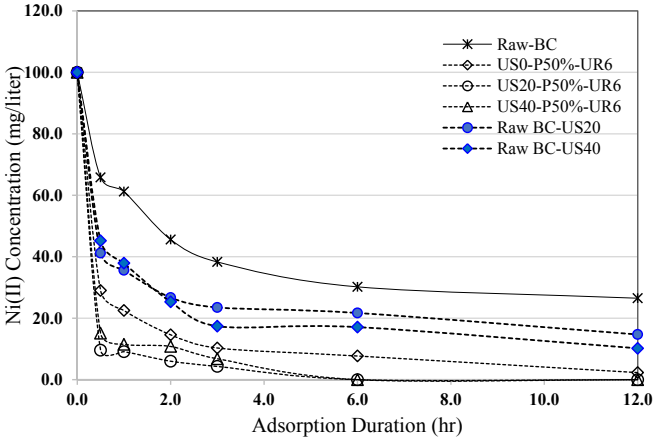

Fig. 9. The effect of ultrasound duration during functionalization on adsorption of Ni(II) by urea functionalized biochar.

There is a lot of intensity above 2500 cm^{-1} in some of the samples which suggested the presence of NH, CH, or OH bands as per the IR and elemental analysis. In addition, the I_D/I_G ratio just slightly changed from 0.821–0.793 to 0.963–0.816 for urea concentrations of 1, 3, 6, and 10 M (with 20 s of ultrasound and 50% phosphoric acid), respectively. On the other hand, elemental analysis showed that carbon content reduced with urea concentration up to 6 M, while ash and nitrogen contents increased. Therefore, a part of the reason for the highest I_D/I_G ratio for US20-P50-U6M may be related to interaction of urea with the oxygen (or phosphorous) containing functional groups that existed on the surface. Urea could become directly attached to the structure, causing a significant increase in I_D/I_G with using urea concentrations of up to 6 M. The reduction of I_D/I_G in the case with the highest urea molarity needs more analysis. It could be due to the significant reductive ability of urea and the removal of O-containing groups, generating less-defective graphene sheets.

3.4. Adsorption studies

3.4.1. Effect of ultrasound irradiation

Physical adsorption, which dramatically affects the performance of biochars, depends on their porous structure. As per SEM images as well as the other analysis, ultrasonication affected the physical structure of biochar. Once induced by ultrasound, biochar was enhanced in its surface area and porosity. Using ultrasound to clean and expand graphite, which has a similar carbon structure to biochar, has been proven successful [13,49]. Ultrasound treatment of graphite and crystalline materials decreases their granularity, meaning breaking apart of irregular-shaped biochar (as per particle size analysis) and creating smoother surfaces (as per SEM images).

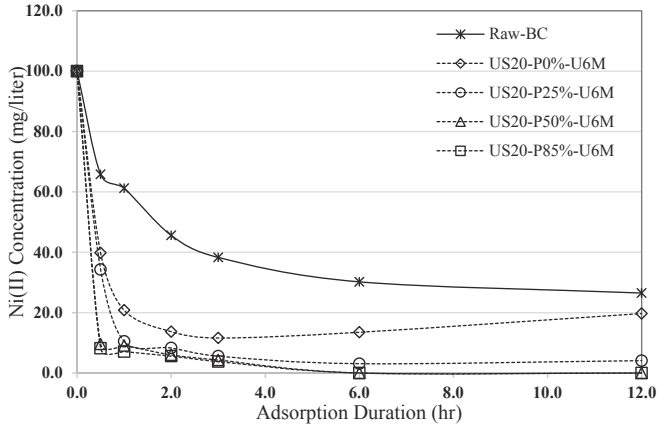

Fig. 10. The effect of phosphoric acid during functionalization on adsorption of Ni(II) by urea functionalized biochar.

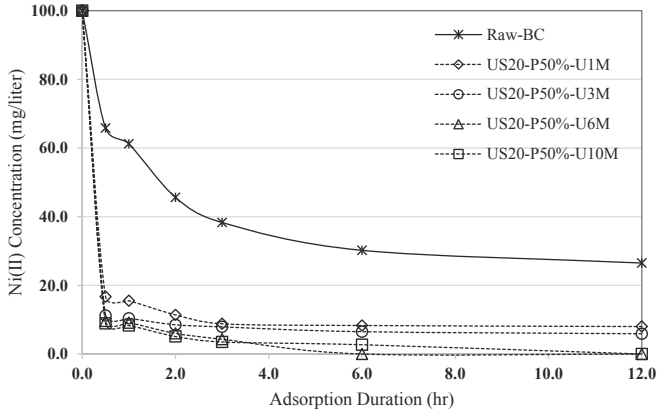

Fig. 11. The effect of urea concentration during functionalization on adsorption of Ni(II) by urea functionalized biochar.

Fig. 9 shows the effect of ultrasound treatment alone for 20 or 40 s, and also its interaction with chemical functionalization, on biochar activity towards the removal of Ni(II). Expectedly, ultrasound irradiation roughly doubled the adsorption capacity of biochar thorough changes in biochar structure, but it still could not remove Ni(II) completely after 12 h. BC and US-BC contained an accessible pore area for metal ions adsorption because their pore sizes were in the range of 0.6–2.3 nm which was large enough compared with the 0.7 Å Ni^{2+} ion radii. Moreover, 40 s of ultrasound slightly yielded better adsorption (90%) after 12 h compared with 20 s (85%). On the other hand, chemical functionalization of biochar without ultrasound showed better results than ultrasound alone, but could not remove > 97% of metal even after 12 h. However, the combination of chemical functionalization with ultrasound treatment of either duration resulted in complete removal of Ni(II) within 6 h. In terms of economic analysis, ultrasonication with the durations of 20 and 40 s consumed 1787 and 3583 J total energy (Table 2). Hence, the shorter sonication time was applied for treating all subsequent samples.

3.4.2. Effect of phosphoric acid

Fig. 10 shows the effect of phosphoric acid concentration on adsorption capacity of the modified biochar. Treatment with ultrasound and urea even without phosphoric acid gave a biochar that adsorbed Ni (II) much better than raw biochar. However, a sign of leaching was observed in longer durations as the [Ni(II)] increased, clarifying the important role of H_3PO_4 treatment in this process. When 25% phosphoric acid was added, the Ni(II) removal was faster and more complete, with no leaching of adsorbed Ni(II). With 50% phosphoric acid, removal was > 99% after 6 h. There was no advantage of increasing to 85% H_3PO_4. This was consistent with the elemental analysis that showed that 50% H_3PO_4 contributed in attaching more amine groups to the biochar, but 85% H_3PO_4 did not give rise to higher %N.

3.4.3. Effect of urea molarity

The abilities of raw and the modified biochars with 20 s of ultrasound, 50% H_3PO_4, and different urea concentrations to remove Ni(II) from an aqueous solution are demonstrated in Fig. 11. Gradual increase of Ni(II) uptake with respect to urea loading on the modified biochar again emphasized the role of amino groups in enhancing both adsorption rate and capacity. The modified samples removed more than 92% of Ni(II) within 6 h, while the raw biochar could only remove 70% over the same time, or 73.5% after 12 h. Biochar modified with 1 M or 3 M urea seemed to saturate their adsorption ability after 3 h, at about 90%.

Table 5
Removal of nickel with biochar.

Biochar-	Synthesis Temp (°C)	Activation	Initial Conc. (mg/L)	Adsorption Duration (h)	Maximum capacity (mg/g)	Ref
Broiler litter	500	Steam	58.7	24	10.1 (96.4) mM/L	[53]
Alfalfa stems	500	Steam	58.7	24	22.4 (19.7) mM/L	[53]
Switchgrass	500	Steam	58.7	24	42.3 (None) mM/L	[53]
Corn cob	500	Steam	58.7	24	12.3 (13.4) mM/L	[53]
Corn Stover	500	Steam	58.7	24	29.3 (95.8) mM/L	[53]
Guayule bagasse	500	Steam	58.7	24	35.4 (22.4) mM/L	[53]
Guayule shrub	500	Steam	58.7	24	86.6 (3.2) mM/L	[53]
Soybean straw	500	Steam	58.7	24	49.5 (30.0) mM/L	[53]
Digested Dairy Waste	600	Non	0.1 mM	18	0.248 mM/g	[54]
Digested whole sugar beet	600	Non	0.1 mM	24	0.197 mM/g	[54]
Hickory	550	NaOH-70C	100	1–1.5 h	11.2 (53.6)	[55]
A	400	Non	100	6	27.86	[56]
A	600	Non	100	6	34.84	[56]
Wheat straw	600	Non	100	6	17.67	[56]
Date Seed biochar	–	Non	1 mM	~6	35.74	[57]
Wheat straw	550	Non	5 mM Ni $(NO_3)_2$	5 min	0.215 mM/g 39.2	[58]
Waste apricot (AC)	–	K_2CO_3-500	10	1 h	22.47	[59]
Waste apricot (AC)	–	K_2CO_3-600	10	1 h	19.37	[59]
Pinewood	550	Non	100	12	73.5	This study
Pinewood	550	Non	100	1	38.8	This study
Pinewood	550	US-P-U	100	1	90.9	This study

A: maize silage 55%, straw 15%, sugar beet bagasse 15%, fruit pomace 10%, manure 5%.
*: the values inside the parentheses shows the adsorption of activated biochar.

Biochar activated with 50% phosphoric acid and 6 M urea could remove 99.99% of nickel within 6 h. Therefore, it can be concluded that the 6 M urea and 50% phosphoric acid, along with 20 s of ultrasonication, provided an efficient, fast, and complete adsorption capacity (See Table 5).

4. Conclusion

Heavy metals in drinking water from the corrosion of piping are increasingly becoming a health hazard for humans. The adsorption and removal of such ions is normally achieved at a high cost. Biochar, a valuable by-product of thermal decomposition of biomass, is known for its porosity and ability to adsorb many materials, elements, and ions while also being affordable. In this study, biochar was physically modified by low frequency ultrasound irradiation, treated by H_3PO_4, and functionalized by urea. This allowed the modified biochar to adsorb the Ni(II) ion from water. The biochar surface area and porosity increased with ultrasound application but decreased when functionalized with urea. However, the synergistic interaction of ultrasound in increasing the surface area and porosity with urea functionalization in attaching amine groups onto the biochar surface remarkably increased the adsorption of Ni(II). As tested, the most efficient biochar was the one physically activated by 20 s of ultrasound irradiation, chemically activated by phosphoric acid of 50%, and functionalized with urea of 6 M. From a solution of 100 mg/L of Ni(II), > 99% adsorption was achieved within 6 h. This method of optimized engineering of biochars can be used to rid drinking and waste water of unwanted heavy metal. Activation of biochar using ultrasound at room temperature for a very short duration (20 s) and using urea as a cheap, facile single-source molecule is economically comparable with current activation processes which usually need temperatures as high as 973–1173 K for at least 2 h.

Acknowledgements

The authors are grateful for the financial support of the National Science Foundation (NSF EPSCoR RII Grant No. OIA-1632899 and MRI Grant No. CHE-1532079). The author also appreciates the UM Science, Technology, Engineering, and Math Summer Research Experience for Undergraduates (STEMS REU) Program at the University of Mississippi.

Appendix A. Supplementary data

Supplementary data to this article can be found online at https://doi.org/10.1016/j.ultsonch.2018.09.015.

References

[1] H. Marsh, F. Rodríguez Reinoso, Activated Carbon, Elsevier, Netherland, 2006.
[2] C.W. Sweitzer, K.A. Burgess, F. Lyon, The chemistry of carbon black in rubber reinforcement, Rubber Chem. Technol. 34 (1961) 709–728.
[3] H.P. Boehm, Chemical identification of surface groups, Adv. Catal. 16 (1966) 179–274.
[4] F.R. Oliveira, A.K. Patel, D.P. Jaisi, S. Adhikari, H. Lu, S.K. Khanal, Environmental application of biochar: current status and perspectives, Bioresour. Technol. (2017).
[5] A.K. Meena, G.K. Mishra, P.K. Rai, C. Rajagopal, P.N. Nagar, Removal of heavy metal ions from aqueous solutions using carbon aerogel as an adsorbent, J. Hazard. Mater. 122 (2005) 161–170.
[6] G. Abdul, X. Zhu, B. Chen, Structural characteristics of biochar-graphene nanosheet composites and their adsorption performance for phthalic acid esters, Chem. Eng. J. 319 (2017) 9–20.
[7] F. Chemat, N. Rombaut, A.-G. Sicaire, A. Meullemiestre, A.-S. Fabiano-Tixier, M. Abert-Vian, Ultrasound assisted extraction of food and natural products. Mechanisms, techniques, combinations, protocols and applications. A review, Ultrason. Sonochem. 34 (2017) 540–560.
[8] M. Wang, Y. Zhang, C. Cai, J. Tu, X. Guo, D. Zhang, Sonoporation-induced cell membrane permeabilization and cytoskeleton disassembly at varied acoustic and microbubble-cell parameters, Sci. Rep. 8 (2018) 3885.
[9] X. Guo, C. Cai, G. Xu, Y. Yang, J. Tu, P. Huang, D. Zhang, Interaction between cavitation microbubble and cell: a simulation of sonoporation using boundary element method (BEM), Ultrason. Sonochem. 39 (2017) 863–871.
[10] M.A. Khayamian, M. Baniassadi, M. Abdolahad, Monitoring the effect of sonoporation on the cells using electrochemical approach, Ultrason. Sonochem. 41 (2018) 619–625.
[11] S. Cheng, L. Zhang, H. Xia, J. Peng, J. Shu, C. Li, Ultrasound and microwave-assisted preparation of Fe-activated carbon as an effective low-cost adsorbent for dyes wastewater treatment, RSC Adv. 6 (2016) 78936–78946.
[12] S. Stankovich, D.A. Dikin, G.H. Dommett, K.M. Kohlhaas, E.J. Zimney, E.A. Stach, R.D. Piner, S.T. Nguyen, R.S. Ruoff, Graphene-based composite materials, Nature 442 (2006) 282–286.
[13] S. Stankovich, R.D. Piner, X. Chen, N. Wu, S.T. Nguyen, R.S. Ruoff, Stable aqueous dispersions of graphitic nanoplatelets via the reduction of exfoliated graphite oxide in the presence of poly(sodium 4-styrenesulfonate), J. Mater. Chem. 16 (2006) 155–158.
[14] F. Guittonneau, A. Abdelouas, B. Grambow, S. Huclier, The effect of high power ultrasound on an aqueous suspension of graphite, Ultrason. Sonochem. 17 (2010) 391–398.
[15] W.-Y. Chen, D.L. Mattern, E. Okinedo, J.C. Senter, A.A. Mattei, C.W. Redwine, Photochemical and acoustic interactions of biochar with CO_2 and H_2O: Applications in power generation and CO_2 capture, AIChE J. 60 (2014) 1054–1065.
[16] H. Yang, H. Li, J. Zhai, L. Sun, H. Yu, Simple synthesis of graphene oxide using ultrasonic cleaner from expanded graphite, Ind. Eng. Chem. Res. 53 (2014) 17878–17883.
[17] S.B.A. Hamid, Z.Z. Chowdhury, S.M. Zain, Base catalytic approach: a promising technique for the activation of biochar for equilibrium sorption studies of copper, Cu(II) ions in single solute system, Materials 7 (2014) 2815–2832.
[18] R. Chintala, T.E. Schumacher, S. Kumar, D.D. Malo, J.A. Rice, B. Bleakley, G. Chilom, D.E. Clay, J.L. Julson, S.K. Papiernik, Z.R. Gu, Molecular characterization of biochars and their influence on microbiological properties of soil, J. Hazard. Mater. 279 (2014) 244–256.
[19] C. Wan, Y. Jiao, J. Li, Core-shell composite of wood-derived biochar supported MnO2 nanosheets for supercapacitor applications, RSC Adv. 6 (2016) 64811–64817.
[20] M. Myglovets, O.I. Poddubnaya, O. Sevastyanova, M.E. Lindström, B. Gawdzik, M. Sobiesiak, M.M. Tsyba, V.I. Sapsay, D.O. Klymchuk, A.M. Puziy, Preparation of carbon adsorbents from lignosulfonate by phosphoric acid activation for the adsorption of metal ions, Carbon 80 (2014) 771–783.
[21] R. Yang, G. Liu, X. Xu, M. Li, J. Zhang, X. Hao, Surface texture, chemistry and adsorption properties of acid blue 9 of hemp (*Cannabis sativa* L.) bast-based activated carbon fibers prepared by phosphoric acid activation, Biomass Bioenergy 35 (2011) 437–445.
[22] S.M. Taha, M.E. Amer, A.E. Elmarsafy, M.Y. Elkady, Adsorption of 15 different pesticides on untreated and phosphoric acid treated biochar and charcoal from water, J. Environ. Chem. Eng. 2 (2014) 2013–2025.
[23] D.C.W. Tsang, J. Hu, M.Y. Liu, W. Zhang, K.C.K. Lai, I.M.C. Lo, Activated carbon produced from waste wood pallets: adsorption of three classes of dyes, Water Air Soil Pollut. 184 (2007) 141–155.
[24] X. Sun, P. Cheng, H. Wang, H. Xu, L. Dang, Z. Liu, Z. Lei, Activation of graphene aerogel with phosphoric acid for enhanced electrocapacitive performance, Carbon 92 (2015) 1–10.
[25] A.M. Puziy, O.I. Poddubnaya, A. Martínez-Alonso, F. Suárez-García, J.M.D. Tascón, Synthetic carbons activated with phosphoric acid: I. Surface chemistry and ion binding properties, Carbon 40 (2002) 1493–1505.
[26] M. Uchimiya, S. Chang, K.T. Klasson, Screening biochars for heavy metal retention in soil: role of oxygen functional groups, J. Hazard. Mater. 190 (2011) 432–441.
[27] X. Xu, X. Cao, L. Zhao, Comparison of rice husk- and dairy manure-derived biochars for simultaneously removing heavy metals from aqueous solutions: role of mineral components in biochars, Chemosphere 92 (2013) 955–961.
[28] H. Peng, P. Gao, G. Chu, B. Pan, J. Peng, B. Xing, Enhanced adsorption of Cu(II) and Cd(II) by phosphoric acid-modified biochars, Environ. Pollut. 229 (2017) 846–853.
[29] Y. Lin, P. Munroe, S. Joseph, R. Henderson, A. Ziolkowski, Water extractable organic carbon in untreated and chemical treated biochars, Chemosphere 87 (2012) 151–157.
[30] M. Zakeri, E. Abouzari-lotf, M. Miyake, S. Mehdipour-Ataei, K. Shameli, Phosphoric acid functionalized graphene oxide: a highly dispersible carbon-based nanocatalyst for the green synthesis of bio-active pyrazoles, Arab. J. Chem. (2017).
[31] S. Some, I. Shackery, S.J. Kim, S.C. Jun, Phosphorus-doped graphene oxide layer as a highly efficient flame retardant, Chem. Eur. J. 21 (2015) 15480–15485.
[32] H.Z. Lecher, T.H. Chao, K.C. Whitehouse, R.A. Greenwood, The phosphonation of aromatic compounds with phosphoric anhydride1, J. Am. Chem. Soc. 76 (1954) 1045–1051.
[33] R. Fu, Y. Liu, Z. Lou, Z. Wang, S.A. Baig, X. Xu, Adsorptive removal of Pb(II) by magnetic activated carbon incorporated with amino groups from aqueous solutions, J. Taiwan Inst. Chem. Eng. 62 (2016) 247–258.
[34] Z. Guo, X. Zhang, Y. Kang, J. Zhang, Biomass-derived carbon sorbents for Cd(II) removal: activation and adsorption mechanism, ACS Sustainable Chem. Eng. 5 (2017) 4103–4109.
[35] W. Naowanon, R. Chueachot, S. Klinsrisuk, S. Amnuaypanich, Biphasic synthesis of amine-functionalized mesoporous silica nanospheres (MSN-NH_2) and its application for removal of ferrous (Fe^{2+}) and copper (Cu^{2+}) ions, Powder Technol. 323 (2018) 548–557.
[36] Y. Kang, Z. Guo, J. Zhang, H. Xie, H. Liu, C. Zhang, Enhancement of Ni(II) removal by urea-modified activated carbon derived from Pennisetum alopecuroides with phosphoric acid activation, J. Taiwan Inst. Chem. Eng. 60 (2016) 335–341.
[37] J. Aguado, J.M. Arsuaga, A. Arencibia, M. Lindo, V. Gascón, Aqueous heavy metals removal by adsorption on amine-functionalized mesoporous silica, J. Hazard. Mater. 163 (2009) 213–221.
[38] S.K. Das, A.R. Das, A.K. Guha, A study on the adsorption mechanism of mercury on

aspergillus versicolor biomass, Environ. Sci. Technol. 41 (2007) 8281–8287.
[39] H. Khojasteh, M. Salavati-Niasari, H. Safajou, H. Safardoust-Hojaghan, Facile reduction of graphene using urea in solid phase and surface modification by N-doped graphene quantum dots for adsorption of organic dyes, Diamand Relat. Mater. 79 (2017) 133–144.
[40] X. Xu, Y. Zhou, T. Yuan, Y. Li, Methanol electrocatalytic oxidation on Pt nanoparticles on nitrogen doped graphene prepared by the hydrothermal reaction of graphene oxide with urea, Electrochim. Acta 112 (2013) 587–595.
[41] M.E. Mahmoud, M.A. Khalifa, Y.M. El Wakeel, M.S. Header, T.M. Abdel-Fattah, Engineered nano-magnetic iron oxide-urea-activated carbon nanolayer sorbent for potential removal of uranium (VI) from aqueous solution, J. Nucl. Mater. 487 (2017) 13–22.
[42] P. Chamoli, M.K. Das, K.K. Kar, Urea-assisted low temperature green synthesis of graphene nanosheets for transparent conducting film, J. Phys. Chem. Solids 113 (2018) 17–25.
[43] G. Bekiaris, C. Peltre, L.S. Jensen, S. Bruun, Using FTIR-photoacoustic spectroscopy for phosphorus speciation analysis of biochars, Spectrochim. Acta, Part A 168 (2016) 29–36.
[44] M. Keiluweit, P.S. Nico, M.G. Johnson, M. Kleber, Dynamic molecular structure of plant biomass-derived black carbon (Biochar), Environ. Sci. Technol. 44 (2010) 1247–1253.
[45] N. Claoston, A.W. Samsuri, M.H.A. Husni, M.S.M. Amran, Effects of pyrolysis temperature on the physicochemical properties of empty fruit bunch and rice husk biochars, Waste Manage. Res. 32 (2014) 331–339.
[46] B. Peng, L. Chen, C. Que, K. Yang, F. Deng, X. Deng, G. Shi, G. Xu, M. Wu, Adsorption of antibiotics on graphene and biochar in aqueous solutions induced by π-π interactions, Sci. Rep. 6 (2016) 31920.
[47] Y. Sun, J.P. Zhang, C. Wen, L. Zhang, An enhanced approach for biochar preparation using fluidized bed and its application for H2S removal, Chem. Eng. Process. Process Intensif. 104 (2016) 1–12.
[48] A.C. Ferrari, Raman spectroscopy of graphene and graphite: disorder, electron–phonon coupling, doping and nonadiabatic effects, Solid State Commun. 143 (2007) 47–57.
[49] S. Stankovich, D.A. Dikin, G.H.B. Dommett, K.M. Kohlhaas, E.J. Zimney, E.A. Stach, R.D. Piner, S.T. Nguyen, R.S. Ruoff, Graphene-based composite materials, Nature 442 (2006) 282–286.
[50] Y.K.H. Environmental Engineering, Robert W. Peters, School of Civil Engineering, Evaluation of recent treatment techniques for removal of heavy metals from industrial wastewaters, American Industrial Chemical Engineering Symposium Series, 1985.
[51] S.E. Mansour, I.H. Hasieb, Removal of nickel from drinking water by electro-coagulation technique using alternating current, Curr. Res. Chem. 4 (2012) 41–50.
[52] V.K.R. Dimple Lakherwal, H.P. Singh, Studies on adsorption of nickel by activated carbon in a liquid fluidised bed reactor, Can. Chem. Trans. 4 (2016) 121–132.
[53] I. Lima, A. Boateng, K. Klasson, Physicochemical and adsorptive properties of fast-pyrolysis bio-chars and their steam activated counterparts, 2010.
[54] M. Inyang, B. Gao, Y. Yao, Y. Xue, A.R. Zimmerman, P. Pullammanappallil, X. Cao, Removal of heavy metals from aqueous solution by biochars derived from anaerobically digested biomass, Bioresour. Technol. 110 (2012) 50–56.
[55] Z. Ding, X. Hu, Y. Wan, S. Wang, B. Gao, Removal of lead, copper, cadmium, zinc, and nickel from aqueous solutions by alkali-modified biochar: batch and column tests, J. Ind. Eng. Chem. 33 (2016) 239–245.
[56] A. Bogusz, K. Nowak, M. Stefaniuk, R. Dobrowolski, P. Oleszczuk, Synthesis of biochar from residues after biogas production with respect to cadmium and nickel removal from wastewater, J. Environ. Manage. 201 (2017) 268–276.
[57] Z. Mahdi, A. El Hanandeh, Q. Yu, Date seed derived biochar for Ni(II) removal from aqueous solutions, MATEC Web Conf. 120 (2017) 05005.
[58] Z. Shen, Y. Zhang, O. McMillan, F. Jin, A. Al-Tabbaa, Characteristics and mechanisms of nickel adsorption on biochars produced from wheat straw pellets and rice husk, Environ. Sci. Pollut. Res. 24 (2017) 12809–12819.
[59] S. Erdoğan, Y. Önal, C. Akmil-Başar, S. Bilmez-Erdemoğlu, Ç. Sarıcı-Özdemir, E. Köseoğlu, G. İçduygu, Optimization of nickel adsorption from aqueous solution by using activated carbon prepared from waste apricot by chemical activation, Appl. Surf. Sci. 252 (2005) 1324–1331.